

## Designing Simple Tridentate Ligands for Highly Luminescent Europium Complexes

Nail M. Shavaleev,<sup>[a]</sup> Svetlana V. Eliseeva,<sup>[a]</sup> Rosario Scopelliti,<sup>[a]</sup> and Jean-Claude G. Bünzli\*<sup>[a, b]</sup>

**Abstract:** A series of tridentate benzimidazole-substituted pyridine-2-carboxylic acids have been prepared with a halogen, methyl or alkoxy group in the 6-position of the benzimidazole ring, which additionally contains a solubilising *N*-alkyl chain. The ligands form neutral homoleptic nine-coordinate lanthanum, europium and terbium complexes as established from X-ray crystallographic analysis of eight structures. The coordination polyhedron around the lanthanide ion is close to a tricapped trigonal prism with ligands arranged in an up–up–down fashion. The coordinated ligands serve as light-harvesting chromophores in the com-

plexes with absorption maxima in the range 321–341 nm ( $\epsilon = (4.9\text{--}6.0) \times 10^4 \text{ M}^{-1} \text{ cm}^{-1}$ ) and triplet-state energies between 21300 and 18800  $\text{cm}^{-1}$ ; the largest redshifts occur for bromine and electron-donor alkoxy substituents. The ligands efficiently sensitise europium luminescence with overall quantum yields ( $Q_L^{\text{Eu}}$ ) and observed lifetimes ( $\tau_{\text{obs}}$ ) reaching 71% and 3.00 ms, respectively, in the solid state and 52%

and 2.81 ms, respectively, in  $\text{CH}_2\text{Cl}_2$  at room temperature. The radiative lifetimes of the  $\text{Eu}({}^5\text{D}_0)$  level amount to  $\tau_{\text{rad}} = 3.6\text{--}4.6$  ms and the sensitisation efficiency  $\eta_{\text{sens}} = Q_L^{\text{Eu}}(\tau_{\text{rad}}/\tau_{\text{obs}})$  is close to unity for most of the complexes in the solid state and equal to approximately 80% in solution. The photophysical parameters of the complexes correlate with the triplet energy of the ligands, which in turn is determined by the nature of the benzimidazole substituent. Facile modification of the ligands makes them promising for the development of brightly emissive europium-containing materials.

**Keywords:** benzimidazole • europium • luminescence • radiative lifetime • sensitization efficiency • tridentate ligands

### Introduction

Trivalent europium is one of the most intriguing and resourceful lanthanide luminescent ions. Its red emission line

at 610 nm ( ${}^5\text{D}_0 \rightarrow {}^7\text{F}_2$  transition) was first detected by Sir William Crookes in the spectrum of  $\text{Sm}^{\text{III}}$  in 1885 and confirmed by Lecoq de Boisbaudran in 1892; the entire phosphorescence spectrum from both the  ${}^5\text{D}_0$  and  ${}^5\text{D}_1$  levels was subsequently recorded and assigned in 1900 by Demarçais, who a short while later positively identified the new element.<sup>[1]</sup> Some specific emission features of  $\text{Eu}^{\text{III}}$  are responsible for its wide use in photonic applications, namely: 1) the energy gap between the most emissive  ${}^5\text{D}_0$  level and the highest sub-level of the ground state,  ${}^7\text{F}_6$ , is large enough ( $\approx 12000 \text{ cm}^{-1}$ ) to minimise non-radiative de-activations, except when high-energy phonons (i.e., OH or NH) are operative in the inner coordination sphere; in this case, however, the luminescence quenching may be turned into an advantage for the determination of the hydration number;<sup>[2,3]</sup> 2) the lifetime of the  ${}^5\text{D}_0$  level is in the millisecond range and may even reach values up to 14 ms<sup>[4,5]</sup> in inorganic compounds, thus allowing time-resolved detection with simple instrumentation, a definite advantage for analytical applications; 3) depending on the inorganic matrix or organic complex the  $\text{Eu}^{\text{III}}$  ion is embedded into, the emission may be ex-

[a] Dr. N. M. Shavaleev, Dr. S. V. Eliseeva, Dr. R. Scopelliti, Prof. Dr. J.-C. G. Bünzli  
Laboratory of Lanthanide Supramolecular Chemistry  
École Polytechnique Fédérale de Lausanne (EPFL)  
LCSL-BCH 1402, 1015 Lausanne (Switzerland)  
Fax: (+41)21-693-9825  
E-mail: jean-claude.bunzli@epfl.ch

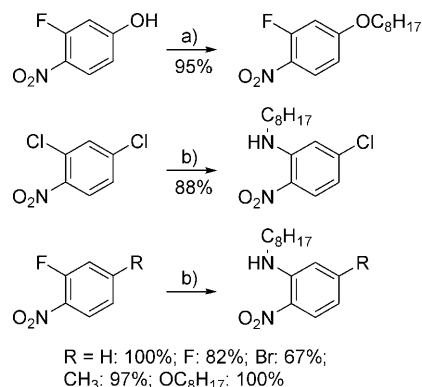
[b] Prof. Dr. J.-C. G. Bünzli  
WCU professor  
Department of Advanced Materials Chemistry and  
Center for Advanced Photovoltaic Materials  
Korea University, 208 Seochang, Jochiwon  
ChungNam 339-700 (South Korea)

Supporting information for this article, which includes synthesis of the ligand precursors and La and Tb complexes;  ${}^1\text{H}$  NMR spectra, absorption and luminescence spectra; and CIF files of the crystal structures, is available on the WWW under <http://dx.doi.org/10.1002/chem.200901996>.



## Results and Discussion

**Synthetic aspects:** The ligands have been synthesised in three steps from 2-carboxaldehyde-6-hydroxymethylpyridine and substituted *o*-nitroanilines (Scheme 1). An efficient synthesis of the former intermediate has been recently described by our group,<sup>[36]</sup> whereas the latter are available by means of a facile reaction of primary alkylamines with 2-halono-benzenes in dimethylsulfoxide (DMSO; Scheme 2). In



Scheme 2. Synthesis of precursors. Reaction conditions: a) 1-octylbromide, K<sub>2</sub>CO<sub>3</sub>, dry DMF, under N<sub>2</sub>, 80 °C; b) *n*-octylamine (excess, used as a reagent and as a base), dry DMSO, under N<sub>2</sub>, heating.

the first step, the benzimidazole ring was formed by reacting 2-carboxaldehyde-6-hydroxymethylpyridine with *o*-nitroaniline in the presence of Na<sub>2</sub>S<sub>2</sub>O<sub>4</sub> in 2-methoxyethanol/H<sub>2</sub>O.<sup>[37]</sup> In the second step, a hydroxymethylpyridine was oxidised to a carboxaldehyde with SeO<sub>2</sub> in dioxane. Finally, the aldehyde was oxidised with H<sub>2</sub>O<sub>2</sub>/formic acid to yield a carboxylic acid.<sup>[38]</sup> The advantages of this synthetic approach are 1) the easy availability of the starting materials, 2) the efficient formation of the benzimidazole ring under mild conditions, and 3) the selective step-wise oxidation that does not result in degradation of the alkyl groups or in *N*-oxide formation. At least two convenient attachment points are available for subsequent grafting of the ligands with functional groups (e.g., chromophore or charge transport), namely, the amine nitrogen on benzimidazole ring and a hydroxyl group of 3-fluoro-4-nitrophenol, which is a precursor to **HL401** and **HL808** (Scheme 2). In addition, a bromine group in ligand **HL8Br** and its precursors offers opportunities for carbon-carbon or carbon-heteroatom coupling.

To test the influence of the substituents on both the formation of the complexes and their photophysical properties, ligands have been prepared that bear electron-acceptor (F, Cl), or electron-donor groups (CH<sub>3</sub>, OCH<sub>3</sub>, OC<sub>8</sub>H<sub>17</sub>), or a 'heavy' atom (Br) at the 6-position of the benzimidazole ring (Scheme 1). Introducing a substituent in this position prevents its steric interference with metal binding while still allowing it to influence the electron density of the coordinating benzimidazole N atom, as a result of the two groups being in *para* configuration. Additionally, variation of the

length of the *N*-alkyl chain allows one to control the solubility of both ligands and complexes.

Complexes with composition [Ln( $\kappa^3$ -ligand)<sub>3</sub>] $\cdot n$ H<sub>2</sub>O ( $n = 0$ – $2$ ; Ln = La, Eu, Tb; abbreviated as **LnLigand**) have been isolated as air- and moisture-stable white solids by reacting the ligand, sodium hydroxide, and lanthanide chloride in 3:3:1 ratio in hot aqueous ethanol (Scheme 1). The complexes containing *N*-methyl or *N*-butyl benzimidazoles are only soluble in DMSO; the ones with longer *N*-octyl chains are also soluble in non-coordinating CH<sub>2</sub>Cl<sub>2</sub>. They have been characterised by elemental analysis (C, H, N), X-ray crystallography, electronic absorption and luminescence spectroscopy. Syntheses of ligands **HL1**, **HL4Me**, their La and Eu complexes, and discussion of their spectroscopic properties have been reported in a preliminary communication.<sup>[32]</sup>

**Structural characterisation of the complexes:** Single crystals suitable for X-ray analysis could be obtained for [Ln(**L1**)<sub>3</sub>], [Ln(**L4Me**)<sub>3</sub>] (Ln = La, Eu, Tb) and [Ln(**L401**)<sub>3</sub>] (Ln = La, Eu); their molecular structures are shown in Figure 1 and selected parameters are collected in Table 1.

All of the complexes share similar structural properties. The lanthanide ion is 9-coordinated by three ligands and its coordination polyhedron can be described as a distorted tri-capped trigonal prism (TCTP, Figure 2),<sup>[39]</sup> with N(py) (py = pyridine) atoms in capping positions and forming a plane with Ln. Two triangular faces of the prism are defined by O-N(b)-N(b) and O-O-N(b) atoms (b = benzimidazole). Each of the three ligands spans both triangular faces of the TCTP through a capping position. However, the complex lacks C<sub>3</sub> symmetry as the ligands are arranged in an up-up-down fashion around the metal. The crystal structures of [Ln(**L4Me**)<sub>3</sub>] (Ln = La, Tb) contain two independent molecules with slightly different metal-ligand bond lengths.

The coordinated ligands are generally not planar with dihedral angles between pyridine and benzimidazole in the range of 2–40°. They are not equally strongly bonded to the metal ion, as reflected in the different respective sets of bond lengths that decrease in the order La > Eu  $\approx$  Tb as a result of lanthanide contraction. The metal ion is preferentially bound to the pyridine-2-carboxylate, whereas bonding to the benzimidazole is relatively weak, which is reflected in longer bond lengths, Ln–O < Ln–N(py) < Ln–N(b), and in their wider variation. Within a complex, the distribution of bond lengths is surprisingly uniform for pyridine compared to carboxylate with  $\Delta = 0.004$ – $0.060$  Å for Ln–N(py), 0.018–0.127 Å for Ln–O and 0.072–0.283 Å for Ln–N(b) (Table 1).

In all **LnL1** structures, two of the ligands are likely to be involved in an intra-complex stacking interaction, as their imidazole rings are nearly parallel and partially overlap with distances of approximately 3.5 Å (Figure 1A–C). The co-crystallised water molecule in **LnL401** forms a hydrogen bond with the carbonyl oxygen of a carboxylate group with O $\cdots$ O(water) = 2.781(5) Å for La and 2.791(10) for Eu; however, the Ln $\cdots$ O(water) distances are >7.1 Å and preclude interaction between them. The structure of **TbL4Me** con-

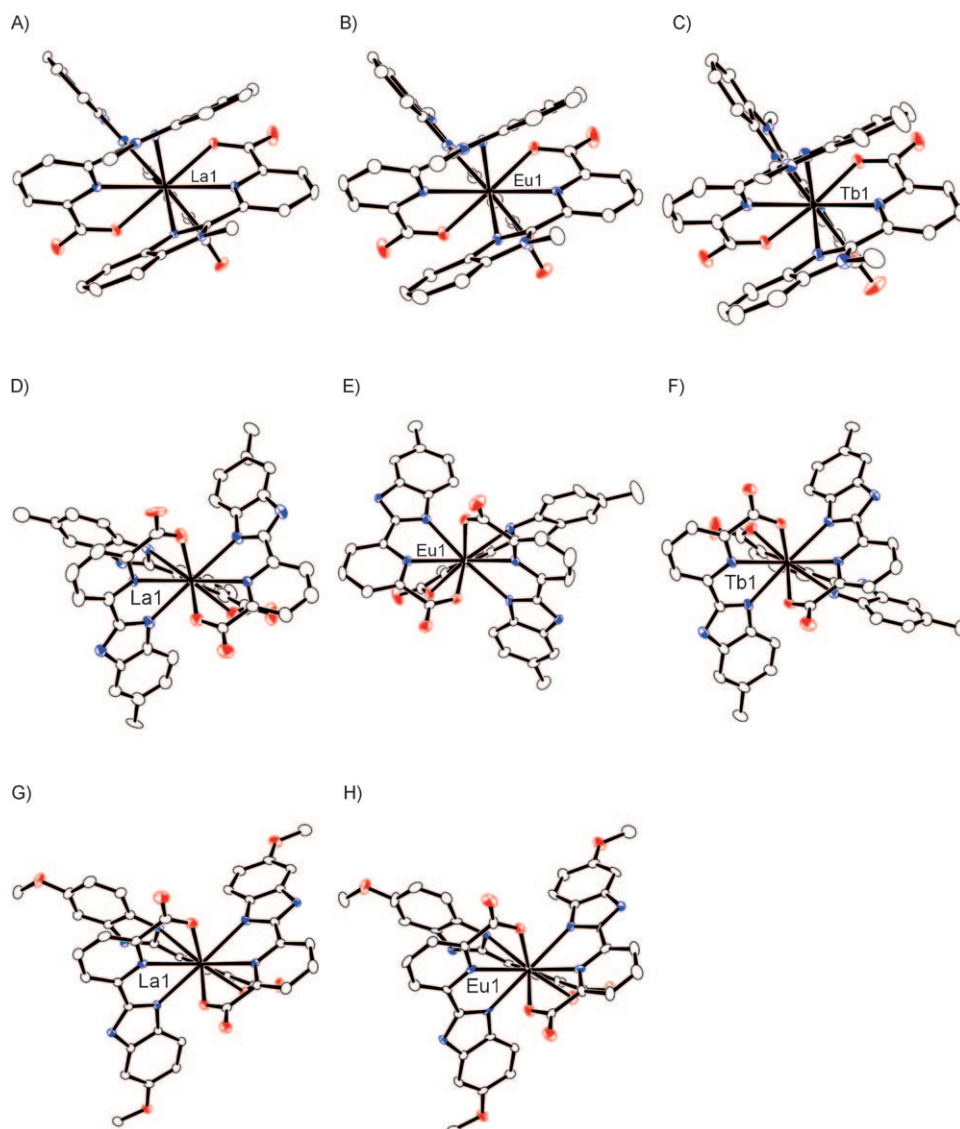


Figure 1. Molecular structures of the lanthanide complexes (50% probability ellipsoids; H atoms, *N*-butyl groups and co-crystallised solvent molecules omitted). Heteroatoms: O, red; N, blue; Ln, black. A–C) **LnL1** (Ln=La, Eu, Tb). D–F) **LnL4Me** (Ln=La, Eu, Tb). G, H) **LnL4O1** (Ln=La, Eu). Only one of the two independent molecules is shown for **LaL4Me** and **TbL4Me**.

tains four co-crystallised water molecules that form three hydrogen bonds with two independent molecules of the complex. The interaction with the first complex consists of a bond to a carbonyl group with  $O\cdots O(\text{water})=2.865 \text{ \AA}$  and  $Tb1\cdots O(\text{water})=7.169 \text{ \AA}$ . For the other complex there are bonds to 1) the hydroxy group of one ligand with  $O\cdots O(\text{water})=2.774 \text{ \AA}$  and a short  $Tb2\cdots O(\text{water})$  distance of  $4.643 \text{ \AA}$ , which may allow interaction between  $Tb^{III}$  and water; and 2) a carbonyl of another ligand with  $O\cdots O(\text{water})=2.778 \text{ \AA}$  and  $Tb2\cdots O(\text{water})=6.986 \text{ \AA}$ . Finally, the inter-metal distances in the structures are  $>9.3 \text{ \AA}$ , which is likely to prevent intermetallic interaction, an a priori favourable situation for luminescent properties.

The relative bonding strengths of the ligands have been quantified with the bond-valence method<sup>[40]</sup> wherein a

donor atom  $j$  lying at a distance  $d_{Ln,j}$  from the metal ion is characterised by a bond-valence contribution  $v_{Ln,j}$  [Eq. (2)]:

$$v_{Ln,j} = e^{(R_{Ln,j} - d_{Ln,j})/b} \quad (2)$$

in which  $R_{Ln,j}$  are the bond-valence parameters for the pair of interacting atoms (Ln–O<sup>[41]</sup> or Ln–N<sup>[42]</sup>), and  $b$  is a constant equal to  $0.37 \text{ \AA}$ . The bond-valence sum (BVS) of the metal ion  $V_{Ln}$  defined by Equation (3) is supposed to match its formal oxidation state if average bond lengths are standard:

$$V_{Ln} = \sum_j v_{Ln,j} \quad (3)$$

As Table 2 shows, the BVS values for the new structures are in the range of 2.85–3.13 and match well the expected value for  $Ln^{III}$  (3.00) within the variability of the method, accepted to be  $\pm 0.25$  valence units, and therefore confirm the good quality of the crystallographic data. For the majority of La and Eu structures,  $BVS=3.01\text{--}3.05$ . The only exception is one of the two independent molecules in **LaL4Me**, which has a slightly larger than expected BVS of 3.13; the lanthanum ion in this complex appears to be on the borderline between 9- and 8-coordination

and exclusion of the longest La–N(b) bond results in  $BVS=2.94$ . For the smaller Tb ion, a consistently lower BVS is calculated (2.85–2.93), which may indicate steric crowding of the ligands resulting in weaker, thus longer bonds. The average contributions from the various coordinating groups are nearly constant and are in the expected series,  $v(O)$ ,  $0.42(4) > v(N(\text{py}))$ ,  $0.31(2) > v(N(b))$ ,  $0.27(6)$ , and very similar to the parameters obtained for a series of Yb–Na binuclear complexes with benzoxazole-substituted 8-hydroxyquinolines.<sup>[20]</sup>

**Ligand-centred electronic states:** UV/Vis absorption spectra of the ligands have been recorded in DMSO, whereas for the complexes, the chosen solvent was non-coordinating  $\text{CH}_2\text{Cl}_2$  (the ligands themselves are insoluble in  $\text{CH}_2\text{Cl}_2$ ).

Table 1. Selected structural parameters of the complexes.<sup>[a]</sup>

|  | Ln–O             | Bond lengths [Å] <sup>[b]</sup> |                   | Angle [°] <sup>[c]</sup><br>py–b | Ln–Ln<br>[Å] <sup>[d]</sup> |
|--|------------------|---------------------------------|-------------------|----------------------------------|-----------------------------|
|  |                  | Ln–N(py)                        | Ln–N(b)           |                                  |                             |
| [La(L1) <sub>3</sub> ]                     | 2.423(4)         | 2.707(5)                        | 2.723(5)          | 2.41                             | 9.391                       |
|  | 2.459(4)         | 2.709(5)                        | 2.796(5)          | 26.64                            |                             |
|  | 2.470(4)         | 2.685(5)                        | 2.785(5)          | 40.28                            |                             |
|  | <b>2.451(20)</b> | <b>2.700(11)</b>                | <b>2.768(32)</b>  | <b>23(16)</b>                    |                             |
|  | <b>0.047</b>     | <b>0.024</b>                    | <b>0.073</b>      | <b>38</b>                        |                             |
| [Eu(L1) <sub>3</sub> ]                     | 2.339(2)         | 2.594(3)                        | 2.632(3)          | 4.10                             | 9.314                       |
|  | 2.355(3)         | 2.585(3)                        | 2.701(3)          | 26.60                            |                             |
|  | 2.357(2)         | 2.555(3)                        | 2.704(3)          | 38.73                            |                             |
|  | <b>2.350(8)</b>  | <b>2.578(17)</b>                | <b>2.679(33)</b>  | <b>23(14)</b>                    |                             |
|  | <b>0.018</b>     | <b>0.039</b>                    | <b>0.072</b>      | <b>35</b>                        |                             |
| [Tb(L1) <sub>3</sub> ]                     | 2.327(3)         | 2.546(3)                        | 2.579(3)          | 12.32                            | 9.534                       |
|  | 2.328(3)         | 2.562(3)                        | 2.673(3)          | 29.27                            |                             |
|  | 2.377(3)         | 2.564(3)                        | 2.682(4)          | 33.29 <sup>[e]</sup>             |                             |
|  |                  |                                 |                   | 26.46 <sup>[e]</sup>             |                             |
|  | <b>2.344(23)</b> | <b>2.557(8)</b>                 | <b>2.645(47)</b>  | <b>25 (8)</b>                    |                             |
| [La(L4Me) <sub>3</sub> ](1) <sup>[f]</sup> | 2.429(11)        | 2.651(12)                       | 2.750(12)         | 20.03                            | 10.128                      |
|  | 2.449(11)        | 2.698(12)                       | 2.588(13)         | 6.48                             |                             |
|  | 2.499(13)        | 2.699(12)                       | 2.871(12)         | 34.35                            |                             |
|  | <b>2.459(29)</b> | <b>2.683(22)</b>                | <b>2.736(116)</b> | <b>20 (11)</b>                   |                             |
|  | <b>0.07</b>      | <b>0.048</b>                    | <b>0.283</b>      | <b>28</b>                        |                             |
| [La(L4Me) <sub>3</sub> ](2) <sup>[f]</sup> | 2.429(11)        | 2.695(13)                       | 2.741(13)         | 8.28                             |                             |
|  | 2.430(10)        | 2.699(12)                       | 2.631(12)         | 20.65                            |                             |
|  | 2.556(11)        | 2.698(12)                       | 2.839(12)         | 36.77                            |                             |
|  | <b>2.472(60)</b> | <b>2.697(2)</b>                 | <b>2.737(85)</b>  | <b>22 (12)</b>                   |                             |
|  | <b>0.127</b>     | <b>0.004</b>                    | <b>0.208</b>      | <b>28</b>                        |                             |
| [Eu(L4Me) <sub>3</sub> ]                   | 2.342(2)         | 2.588(3)                        | 2.564(3)          | 4.28                             | 9.633                       |
|  | 2.365(2)         | 2.588(3)                        | 2.613(3)          | 8.33                             |                             |
|  | 2.393(2)         | 2.604(3)                        | 2.735(3)          | 31.86                            |                             |
|  | <b>2.367(21)</b> | <b>2.593(8)</b>                 | <b>2.637(72)</b>  | <b>15 (12)</b>                   |                             |
|  | <b>0.051</b>     | <b>0.016</b>                    | <b>0.171</b>      | <b>28</b>                        |                             |
| [Tb(L4Me) <sub>3</sub> ](1) <sup>[f]</sup> | 2.336(3)         | 2.576(3)                        | 2.601(4)          | 19.69                            | 10.094                      |
|  | 2.337(3)         | 2.551(4)                        | 2.560(3)          | 6.29                             |                             |
|  | 2.363(3)         | 2.575(4)                        | 2.772(4)          | 31.29                            |                             |
|  | <b>2.345(12)</b> | <b>2.567(12)</b>                | <b>2.644(92)</b>  | <b>19 (10)</b>                   |                             |
|  | <b>0.027</b>     | <b>0.025</b>                    | <b>0.212</b>      | <b>25</b>                        |                             |
| [Tb(L4Me) <sub>3</sub> ](2) <sup>[f]</sup> | 2.332(3)         | 2.564(4)                        | 2.572(3)          | 9.73                             |                             |
|  | 2.337(3)         | 2.551(3)                        | 2.575(4)          | 19.70                            |                             |
|  | 2.430(3)         | 2.596(4)                        | 2.776(3)          | 36.70                            |                             |
|  | <b>2.366(45)</b> | <b>2.570(19)</b>                | <b>2.641(95)</b>  | <b>22 (11)</b>                   |                             |
|  | <b>0.098</b>     | <b>0.045</b>                    | <b>0.204</b>      | <b>27</b>                        |                             |
| [La(L4O1) <sub>3</sub> ]                   | 2.4458(17)       | 2.6726(19)                      | 2.692(2)          | 8.38                             | 9.700                       |
|  | 2.4620(17)       | 2.702(2)                        | 2.7229(19)        | 18.24                            |                             |
|  | 2.4815(18)       | 2.688(2)                        | 2.881(2)          | 33.03                            |                             |
|  | <b>2.463(15)</b> | <b>2.688(12)</b>                | <b>2.765(83)</b>  | <b>20 (10)</b>                   |                             |
|  | <b>0.036</b>     | <b>0.029</b>                    | <b>0.189</b>      | <b>25</b>                        |                             |
| [Eu(L4O1) <sub>3</sub> ]                   | 2.347(4)         | 2.533(5)                        | 2.574(5)          | 7.80                             | 9.647                       |
|  | 2.356(3)         | 2.593(4)                        | 2.592(5)          | 14.31                            |                             |
|  | 2.394(3)         | 2.584(4)                        | 2.808(4)          | 34.19                            |                             |
|  | <b>2.366(20)</b> | <b>2.570(26)</b>                | <b>2.658(106)</b> | <b>19 (11)</b>                   |                             |
|  | <b>0.047</b>     | <b>0.060</b>                    | <b>0.234</b>      | <b>26</b>                        |                             |

[a] Each line in the table corresponds to one and the same ligand in the complex. Numbers in bold are averaged data (with standard deviations  $\sigma$  in the parenthesis); values in bold and in italic are the differences between the minimum and the maximum values. [b] N(py) and N(b) are nitrogen atoms of pyridine and benzimidazole rings, respectively. [c] Dihedral angles between the planes of pyridine and benzimidazole defined by C and N atoms of core rings. [d] The shortest Ln–Ln distance in the structure. [e] Benzimidazole group is disordered over two positions. [f] Two independent molecules are present in the unit cell of these complexes.

The corresponding spectra are shown in Figure 3 and Figures S1–S8 (see the Supporting Information), whereas the main spectral features are summarised in Table 3 and Table S1 (also in the Supporting Information).

The ligands display a composite broad absorption band in the UV range corresponding to  $\pi \rightarrow \pi^*$  transitions with a maximum at 315–331 nm, two shoulders at shorter and longer wavelengths and a cut-off between 350 and 375 nm. The maximum is shifted to lower energies in the order (F, H) > Cl  $\approx$  Br > CH<sub>3</sub> > OCH<sub>3</sub>  $\approx$  OC<sub>8</sub>H<sub>17</sub>. The largest redshift is recorded for electron-donor alkoxy groups ( $\approx$ 17 nm) and can be explained by a contribution of a charge-transfer transition localised on benzimidazole ring wherein the imine moiety acts as an acceptor. The shifts are smaller for the other substituents, <6 nm. The intensity of the band is in the range (2.2–2.6)  $\times$  10<sup>4</sup> M<sup>-1</sup> cm<sup>-1</sup>, and decreases in the order Br > Cl > (OCH<sub>3</sub>, CH<sub>3</sub>) > (OC<sub>8</sub>H<sub>17</sub>, F) > H.

Upon complex formation, the ligand-centred absorption bands sustain redshifts of about 10 nm for the maxima and 10–25 nm for the cut-offs. The wavelengths of the absorption maxima in the complexes follow the trend observed in the free ligands. A small redshift, <3 nm, is observed as lanthanum is substituted by europium. The ligand absorption in the complexes is significant, with the molar absorption coefficient reaching (4.9–6.0)  $\times$  10<sup>4</sup> M<sup>-1</sup> cm<sup>-1</sup>. These features point to the ligands being adequate light-harvesting chromophores for the sensitisation of lanthanide luminescence.

In one of the preferred energy migration paths in lanthanide complexes, excitation energy is funnelled to the metal ion through the long-lived ligand-centred triplet state.<sup>[19,43]</sup> Thus, for a ligand to be a suitable sensitiser, its triplet state should be situated above the Ln emitting level and the energy gap between them is often correlated with the overall quantum yield; too large a gap leads to inefficient transfer, whereas too small a gap results in back trans-

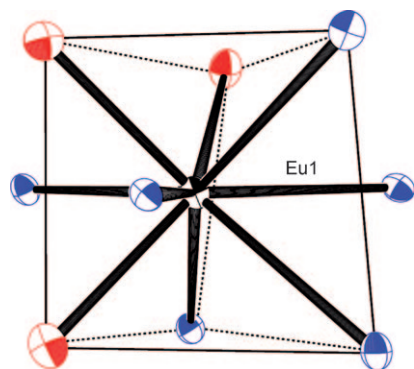


Figure 2. Coordination environment of  $\text{Eu}^{\text{III}}$  in the complex  $[\text{Eu}(\text{L1})_3]$ . Heteroatoms: O, red; N, blue; Eu, black.

Table 2. Calculated bond valence parameters.<sup>[a]</sup>

|   | $V_{\text{Ln}}$ | $\nu_{\text{Ln}}(\text{O})$ | $N(\text{py})$ | $\nu_{\text{Ln}}(\text{N})$ | $N(\text{av.})$ |
|---|-----------------|-----------------------------|----------------|-----------------------------|-----------------|
| $[\text{La}(\text{L1})_3]$                      | 3.01            | 0.44(3)                     | 0.31(1)        | 0.26(3)                     | 0.28(3)         |
| $[\text{Eu}(\text{L1})_3]$                      | 3.01            | 0.43(1)                     | 0.32(1)        | 0.25(2)                     | 0.29(4)         |
| $[\text{Tb}(\text{L1})_3]$                      | 2.93            | 0.41(3)                     | 0.32(1)        | 0.25(3)                     | 0.28(4)         |
| $[\text{La}(\text{L4Me})_3]$ (1) <sup>[b]</sup> | 3.13            | 0.43(3)                     | 0.32(2)        | 0.29(9)                     | 0.31(7)         |
| $[\text{La}(\text{L4Me})_3]$ (2) <sup>[b]</sup> | 3.04            | 0.42(6)                     | 0.31(1)        | 0.28(6)                     | 0.30(5)         |
| $[\text{Eu}(\text{L4Me})_3]$                    | 3.01            | 0.41(2)                     | 0.31(1)        | 0.28(5)                     | 0.30(4)         |
| $[\text{Tb}(\text{L4Me})_3]$ (1) <sup>[b]</sup> | 2.91            | 0.41(1)                     | 0.31(1)        | 0.26(6)                     | 0.28(5)         |
| $[\text{Tb}(\text{L4Me})_3]$ (2) <sup>[b]</sup> | 2.85            | 0.39(5)                     | 0.30(2)        | 0.26(6)                     | 0.28(5)         |
| $[\text{La}(\text{L4O1})_3]$                    | 3.02            | 0.43(2)                     | 0.32(1)        | 0.26(5)                     | 0.29(5)         |
| $[\text{Eu}(\text{L4O1})_3]$                    | 3.05            | 0.41(2)                     | 0.33(2)        | 0.27(7)                     | 0.30(6)         |
| all data  |                 | 0.42(4)                     | 0.31(2)        | 0.27(6)                     | 0.29(5)         |

[a] Averaged bond-valence contribution is listed with standard deviation ( $\sigma$ ) in parentheses. [b] Two independent molecules are present in the unit cell of these complexes.

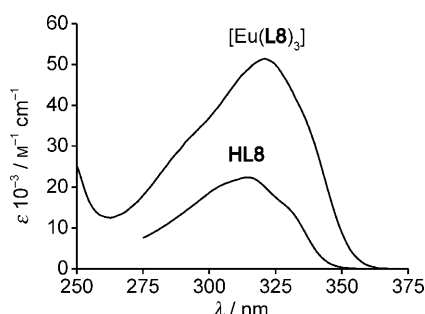


Figure 3. Absorption spectra of ligand **HL8** ( $1.60 \times 10^{-4} \text{ M}$ ) in DMSO and its complex  $[\text{Eu}(\text{L8})_3]$  ( $5.29 \times 10^{-5} \text{ M}$ ) in  $\text{CH}_2\text{Cl}_2$ . All other absorption spectra are similar and are provided in the Supporting Information.

fer.<sup>[43,44]</sup> The phosphorescence spectra of the lanthanum complexes display bands with vibrational spacing on the order of  $1060\text{--}1530 \text{ cm}^{-1}$ , which is attributable to ring-breathing modes (Figure 4, Table 4). The triplet energies of the ligands ( $E_{\text{T}}$ ) have been determined from the zero-phonon transition and are in the range of  $21\,300\text{--}18\,760 \text{ cm}^{-1}$  (Table 4) and decrease as a function of the substituents as  $(\text{H, F, Cl}) > \text{CH}_3 > \text{Br} > \text{OC}_8\text{H}_{17} > \text{OCH}_3$ , that is, roughly following the trend observed in the absorption spectra (Table 3). The largest redshift,  $1800\text{--}2400 \text{ cm}^{-1}$ , is observed for alkoxy-substituted ligands; for others the shift is within

Table 3. Absorption spectra of the ligands in DMSO and their europium complexes in  $\text{CH}_2\text{Cl}_2$ .<sup>[a]</sup>

|                             | $\lambda_{\text{max}}$ [nm] ( $\epsilon$ [ $10^3 \text{ M}^{-1} \text{ cm}^{-1}$ ]) |  |          |
|-----------------------------|---|--|----------|
| <b>HL8</b>                  | 315 (22)  | $[\text{Eu}(\text{L8})_3]$   | 321 (51) |
| <b>HL8F</b>                 | 315 (23)  | $[\text{Eu}(\text{L8F})_3]$  | 322 (52) |
| <b>HL8Cl</b>                | 318 (25)  | $[\text{Eu}(\text{L8Cl})_3]$   | 325 (56) |
| <b>HL8Br</b>                | 319 (26)  | $[\text{Eu}(\text{L8Br})_3]$   | 326 (60) |
| <b>HL8Me</b> <sup>[b]</sup> | 321 (24)  | $[\text{Eu}(\text{L8Me})_3] \cdot 0.5 \text{ H}_2\text{O}$           | 328 (53) |
| <b>HL8O8</b>                | 332 (23)  | $[\text{Eu}(\text{L8O8})_3] \cdot 1.5 \text{ H}_2\text{O}$           | 341 (49) |
| <b>HL4O1</b> <sup>[b]</sup> | 331 (24)  | $[\text{Eu}(\text{L4O1})_3] \cdot \text{H}_2\text{O}$ <sup>[c]</sup> | 336 (56) |

[a] Spectra were recorded at room temperature at  $250\text{--}500 \text{ nm}$ . Estimated errors are  $\pm 1 \text{ nm}$  for  $\lambda_{\text{max}}$  and  $\pm 5\%$  for  $\epsilon$ . Absorption data for  $\text{La}^{\text{III}}$  and  $\text{Tb}^{\text{III}}$  complexes are similar and are provided in Table S1 in the Supporting Information. [b] Elemental analyses correspond to compositions **HL8Me** $\cdot 0.5 \text{ HCO}_2\text{H} \cdot 0.25 \text{ H}_2\text{O}$  and **HL4O1** $\cdot \text{H}_2\text{O}$ , respectively. [c] Recorded in DMSO. The complex is insoluble in  $\text{CH}_2\text{Cl}_2$ ; its  $\epsilon$  has been calculated by assuming that it remains un-dissociated in DMSO.

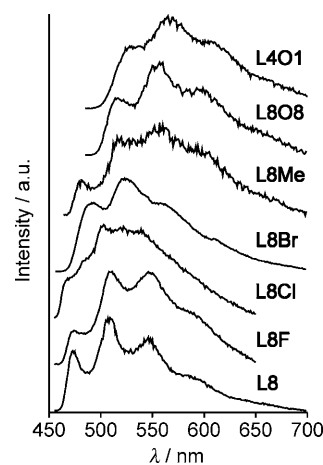


Figure 4. Phosphorescence spectra (corrected and normalised) of lanthanum complexes in the solid state at  $77 \text{ K}$  ( $\lambda_{\text{exc}} = 320\text{--}340 \text{ nm}$ ; emission slit: 5 or  $7 \text{ nm}$ ).

Table 4. Energies of the phonon transitions in the phosphorescence spectra of lanthanum complexes in solid state at  $77 \text{ K}$ .

|  | $E$ [ $\text{cm}^{-1}$ ] |        |          |        |          |
|--|--------------------------|--------|----------|--------|----------|
|  | 0–0                      | 0–1    | $\Delta$ | 0–2    | $\Delta$ |
| $[\text{La}(\text{L8})_3]$                                 | 21 140                   | 19 650 | 1490     | 18 300 | 1350     |
| $[\text{La}(\text{L8F})_3]$                                | 21 100                   | 19 570 | 1530     | 18 300 | 1270     |
| $[\text{La}(\text{L8Cl})_3]$                               | 21 300                   | –      | –        | –      | –        |
| $[\text{La}(\text{L8Br})_3] \cdot 2 \text{ H}_2\text{O}$   | 20 280                   | 19 120 | 1160     | 17 920 | 1200     |
| $[\text{La}(\text{L8Me})_3]$                               | 20 790                   | 19 310 | 1490     | 17 950 | 1360     |
| $[\text{La}(\text{L8O8})_3] \cdot 1.5 \text{ H}_2\text{O}$ | 19 340                   | 17 950 | 1390     | 16 810 | 1140     |
| $[\text{La}(\text{L4O1})_3] \cdot \text{H}_2\text{O}$      | 18 760                   | 17 700 | 1060     | 16 470 | 1230     |

$500 \text{ cm}^{-1}$  apart from a surprisingly low energy for **L8Br**<sup>−</sup> (down by  $860 \text{ cm}^{-1}$ ). With respect to the aim of this work, the energy gap between  $E_{\text{T}}$  and  $^5\text{D}_0$  states is in the  $3900\text{--}1500 \text{ cm}^{-1}$  range, which is an almost ideal situation for sensitisation of  $\text{Eu}^{\text{III}}$  luminescence (Figure 5).

**Europium-centred luminescence:** Under ligand excitation, all europium complexes emit characteristic metal-centred luminescence in the solid state,  $\text{CH}_2\text{Cl}_2$  and under the form of thin film with a thickness of approximately  $50 \text{ nm}$ . The cor-

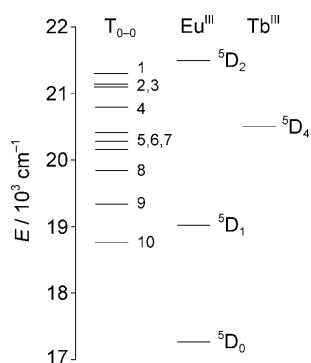


Figure 5. Partial energy diagram of  $\text{Eu}^{\text{III}}$  and  $\text{Tb}^{\text{III}}$  ions, and energy of the ligand-centred triplet states in  $\text{La}^{\text{III}}$  complexes at 77 K; 1) **LaL8Cl**, 2) **LaL8**, 3) **LaL8F**, 4) **LaL8Me**, 5) **LaL4Me**, 6) **LaL8Br**, 7) **LaL1**, 8) **LaLPh**, 9) **LaL8O8**, 10) **LaL4O1**.

responding spectra are shown in Figure 6 and Figures S9–S14 (see the Supporting Information), whereas relevant parameters are listed in Table 5 and Tables S2–S3 (Supporting

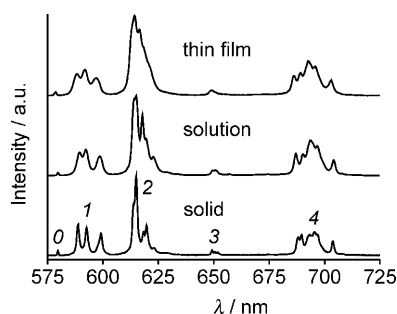


Figure 6. Luminescence spectra (corrected and normalised) of  $[\text{Eu}(\text{L8})_3]$  that display the  $^5\text{D}_0 \rightarrow ^7\text{F}_j$  ( $J=0-4$ ) transitions at room temperature for samples in the solid state,  $8.3 \times 10^{-4} \text{ M}$  in  $\text{CH}_2\text{Cl}_2$ , and as thin film spin-coated on a quartz substrate;  $\lambda_{\text{exc}} = 330 \text{ nm}$ ; emission slit: 0.2 nm (solid) or 0.5 nm. Emission spectra for other europium complexes are similar and are provided in the Supporting Information.

Information). The excitation spectra display prominent ligand bands in the UV range and faint f–f transitions at 395 ( $^5\text{L}_6 \leftarrow ^7\text{F}_{0,1}$ ) and 463 nm ( $^5\text{D}_2 \leftarrow ^7\text{F}_{0,1}$ ), thus confirming the sensitisation of the europium luminescence by the ligands (Figures S15–S16 in the Supporting Information).

The europium-centred emission spectra are similar for all complexes and display sharp bands in the solid state that become broader in solution and more so in the thin film (Figure 6). They are typical of  $\text{Eu}^{\text{III}}$  ions in a low symmetry, pseudo-TCTP environment in accordance with X-ray analysis (Figure 2), with emission intensity fairly equally distributed in the 590–720 nm spectral range. The relative band intensities normalised with respect to the magnetic-dipole  $^5\text{D}_0 \rightarrow ^7\text{F}_1$  transition depend on the medium (Table S2 in the Supporting Information) and the total integrated relative intensity increases by up to 20% in going from the solid state to the solution and to the thin film. The  $^5\text{D}_0 \rightarrow ^7\text{F}_0$  transition is very weak and represents only 0.5% of the total emission.

Table 5. Photophysical parameters of europium and terbium complexes at room temperature.<sup>[a]</sup>

| Complex  |                          | $\tau_{\text{obs}}$<br>[ms] | $Q_{\text{L}}^{\text{Ln}}$<br>[%] | $\tau_{\text{rad}}$<br>[ms] | $Q_{\text{Eu}}^{\text{Eu}}$<br>[%] | $\eta_{\text{sens}}$ |
|--|--------------------------|-----------------------------|-----------------------------------|-----------------------------|------------------------------------|----------------------|
| $[\text{Eu}(\text{L8})_3]$                                 | solid                    | 2.95(2)                     | 71(1)                             | 4.60                        | 64                                 | $\approx 100$        |
|  | $\text{CH}_2\text{Cl}_2$ | 2.76(1)                     | 52(1)                             | 4.39                        | 63                                 | 83                   |
|  | thin film                | 2.46(2)                     | –                                 | 3.64                        | 68                                 | –                    |
| $[\text{Eu}(\text{L8F})_3]$                                | solid                    | 3.00(2)                     | 68(3)                             | 4.42                        | 68                                 | 100                  |
|  | $\text{CH}_2\text{Cl}_2$ | 2.74(2)                     | 51(1)                             | 4.34                        | 63                                 | 81                   |
| $[\text{Eu}(\text{L8Cl})_3]$                               | solid                    | 2.94(3)                     | 71(2)                             | 4.42                        | 67                                 | $\approx 100$        |
|  | $\text{CH}_2\text{Cl}_2$ | 2.71(1)                     | 51(2)                             | 4.35                        | 62                                 | 82                   |
| $[\text{Eu}(\text{L8Br})_3]$                               | solid                    | 2.51(1)                     | 54(1)                             | 4.15                        | 60                                 | 89                   |
|  | $\text{CH}_2\text{Cl}_2$ | 2.73(2)                     | 51(1)                             | 4.28                        | 64                                 | 80                   |
| $[\text{Eu}(\text{L8Me})_3] \cdot 0.5 \text{ H}_2\text{O}$ | solid                    | 2.69(1)                     | 68(4)                             | 4.38                        | 61                                 | $\approx 100$        |
|  | $\text{CH}_2\text{Cl}_2$ | 2.81(1)                     | 52(1)                             | 4.40                        | 64                                 | 81                   |
| $[\text{Eu}(\text{L8O8})_3] \cdot 1.5 \text{ H}_2\text{O}$ | solid                    | 2.45(1)                     | 52(4)                             | 3.88                        | 63                                 | 82                   |
|  | $\text{CH}_2\text{Cl}_2$ | 2.39(2)                     | 42(1)                             | 4.38                        | 55                                 | 77                   |
| $[\text{Eu}(\text{L4O1})_3] \cdot \text{H}_2\text{O}$      | solid                    | 2.93(2)                     | 43(2)                             | 4.48                        | 65                                 | 66                   |
| $[\text{Tb}(\text{L1})_3] \cdot 2 \text{ H}_2\text{O}$     | solid                    | 0.30(2)                     | 9.0(2)                            | –                           | –                                  | –                    |

[a] In the solid state, thin film or  $(6.2\text{--}8.3) \times 10^{-4} \text{ M}$  in  $\text{CH}_2\text{Cl}_2$ .  $\lambda_{\text{exc}} = 330 \text{ nm}$ . Standard deviations ( $2\sigma$ ) are given between parentheses; estimated relative errors:  $\tau_{\text{obs}} \pm 2\%$ ;  $Q_{\text{L}}^{\text{Ln}} \pm 10\%$  (solid state);  $Q_{\text{L}}^{\text{Ln}} \pm 5\%$  (solution);  $\tau_{\text{rad}} \pm 10\%$ ;  $Q_{\text{Eu}}^{\text{Eu}} \pm 12\%$ ;  $\eta_{\text{sens}} \pm 22\%$  (solid state);  $\eta_{\text{sens}} \pm 17\%$  (solution).

The hypersensitive  $^5\text{D}_0 \rightarrow ^7\text{F}_2$  transition is dominant, with  $I(^7\text{F}_2)/I(^7\text{F}_1) = 1.8\text{--}2.7$ , but the  $^5\text{D}_0 \rightarrow ^7\text{F}_4$  transition also has a sizeable intensity, with  $I(^7\text{F}_4)/I(^7\text{F}_1) = 1.4\text{--}1.8$ . Although the relative intensities of the  $^5\text{D}_0 \rightarrow ^7\text{F}_2$  and  $^5\text{D}_0 \rightarrow ^7\text{F}_4$  transitions vary with the complex and the medium, the proportion of light emitted by them with respect to total emission is nearly constant with averages and  $\sigma$  of 45(2) and 35(1)%, respectively.

More insight into the structural properties of **EuL8** and **EuL4Me** has been gained by analyzing the emission spectra of polycrystalline solid-state samples at 10 K and under high resolution (Figure S11 in the Supporting Information). The  $^5\text{D}_0 \rightarrow ^7\text{F}_0$  transition, which is expected to provide a single line for a single coordination environment, does display one extremely narrow component at  $17236 \text{ cm}^{-1}$  for **EuL8** both in the emission (full width at half-height,  $\text{fwhh} = 1.8 \text{ cm}^{-1}$ ) and in the excitation spectra ( $\text{fwhh} = 1.1 \text{ cm}^{-1}$ ), see Figure 7 and Figure S11 in the Supporting Information. The  $^5\text{D}_0 \rightarrow ^7\text{F}_1$  transition of **EuL8** displays three main bands, which is typical of a low-symmetry species; these are further split (Figure 7). A comparison with the IR spectrum points to the

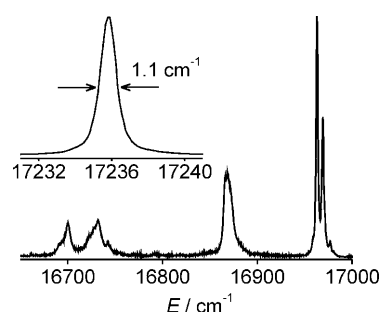


Figure 7. High-resolution emission spectrum of the  $^5\text{D}_0 \rightarrow ^7\text{F}_1$  transition of  $[\text{Eu}(\text{L8})_3]$  at 10 K. Inset: Excitation spectrum of the  $^5\text{D}_0 \rightarrow ^7\text{F}_0$  transition at 10 K.

Fermi-type interaction between the electronic and vibrational states being most likely responsible for the splitting of the high-energy components (Figure S13 in the Supporting Information), as has been reported for an  $\text{Eu}^{\text{III}}$  complex with a crown ether.<sup>[45]</sup> The splitting of the low-energy component is too large for such an interaction, but this transition could be essentially of vibronic nature. Overall, the high-resolution spectrum is consistent with a single-coordination environment of the  $\text{Eu}^{\text{III}}$  ion in **EuL8**. The situation is quite different for **EuL4Me** in that the 0–0 transition is much broader (fwhh  $\approx 7 \text{ cm}^{-1}$ ) and displays two components both in excitation and in emission spectra (in the latter as a shoulder; Figure S14 in the Supporting Information). Each of the equally intense three components of the 0–1 transition is split into two main components with some further fine structure (Figure S15 in the Supporting Information). Therefore, these results indicate that **EuL4Me** contains at least two slightly different europium sites that could arise from its less good crystallinity compared to **EuL8**.

The luminescence decays ( $\tau_{\text{obs}}$ ) are single-exponential functions for all of the complexes in all media. For solid-state samples,  $\tau_{\text{obs}}$  decreases by 15% when the excitation wavelength is changed from 300 to 380 nm; in other media, it is independent of  $\lambda_{\text{exc}}$ . The observed lifetimes are long: 2.45–3.00 ms in the solid state ( $\lambda_{\text{exc}} = 330 \text{ nm}$ ) and 2.71–2.81 ms in solution (2.39 ms for **EuL8O8**; Table 5). They are essentially temperature independent, with  $\tau_{\text{obs}}$  varying by less than 5–10% in going from 300 to 10 K, thereby reflecting the absence of thermally activated deactivation processes, either vibrational or electronic, that is, through LMCT states (Table S3 in the Supporting Information). Therefore, the results of the luminescence lifetime measurements are consistent with the absence of water in the inner coordination sphere of europium and suggest that it is well shielded from non-radiative deactivations in the rigid  $\text{N}_6\text{O}_3$  environment.

**Quantum yields and sensitisation efficiency:** The quantum yields of the ligand-sensitised  $\text{Eu}^{\text{III}}$  luminescence ( $Q_{\text{L}}^{\text{Eu}}$ ) are large and independent of the excitation wavelength. Their values range between 43 and 71% for solid-state samples and between 42 and 52% for solutions in  $\text{CH}_2\text{Cl}_2$  (Table 5). In the solid state, they correlate with the energy of the ligand triplet state, both parameters decreasing in the order (H, F, Cl)  $\approx \text{CH}_3 > \text{Br} > \text{OC}_8\text{H}_{17} > \text{OCH}_3$  (Figure 8). In solution,  $Q_{\text{L}}^{\text{Eu}}$  and  $\tau_{\text{obs}}$  are less sensitive to small changes in triplet-state energy and are essentially constant for all the complexes, apart from the lower values for **EuL8O8** (Figure 8).

The intrinsic quantum yields of  $\text{Eu}^{\text{III}}$  (i.e., measured upon direct f–f excitation) could not be determined experimentally due to very low absorption intensity. Therefore, quantitative analysis of the photophysical parameters has been performed in terms of Equation (1), whereas the radiative lifetimes of  $\text{Eu}({}^5\text{D}_0)$  have been calculated from Equation (4), in which  $n$  is the refractive index (1.5 for solid-state metal–organic complexes; 1.4242 for  $\text{CH}_2\text{Cl}_2$ ),  $A_{\text{MD},0}$  is the spontaneous emission probability for the  ${}^5\text{D}_0 \rightarrow {}^7\text{F}_1$  transition in vacuo

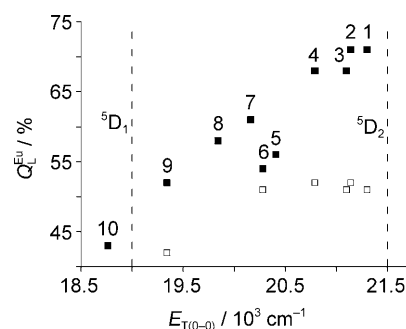


Figure 8. Dependence of the overall quantum yield of europium on the triplet-state energy (at 77 K) of the ligands in the solid state (■) and in  $\text{CH}_2\text{Cl}_2$  (□) at room temperature. The data points have been taken from the present study and from ref. [32]. 1) **EuL8Cl**, 2) **EuL8**, 3) **EuL8F**, 4) **EuL8Me**, 5) **EuL4Me**, 6) **EuL8Br**, 7) **EuL1**, 8) **EuLPh**, 9) **EuL8O8**, 10) **EuL4O1**. The dashed lines indicate the energy of the  ${}^5\text{D}_1$  and  ${}^5\text{D}_2$  levels of europium.

( $14.65 \text{ s}^{-1}$ ), and  $I_{\text{tot}}/I_{\text{MD}}$  is the ratio of the total integrated intensity of the corrected  $\text{Eu}^{\text{III}}$  emission spectrum to the integrated intensity of the magnetic dipole  ${}^5\text{D}_0 \rightarrow {}^7\text{F}_1$  transition (Table S2 in the Supporting Information):<sup>[46]</sup>

$$1/\tau_{\text{rad}} = A_{\text{MD},0} n^3 (I_{\text{tot}}/I_{\text{MD}}) \quad (4)$$

The calculated radiative lifetimes fall into the narrow range of 4.15–4.60 ms in the solid state (3.88 ms for **EuL8O8**) and 4.28–4.40 ms in solution. The intrinsic quantum yields of europium estimated from the ratio  $\tau_{\text{obs}}/\tau_{\text{rad}}$  are large (Table 5), with averages equal to 62(4)% for solid-state samples and 63(1)% for solutions in  $\text{CH}_2\text{Cl}_2$  (55% for **EuL8O8**). Again, the small variation of both the radiative lifetimes and intrinsic quantum yields is to be traced back to the similar  $\text{N}_6\text{O}_3$  coordination environment for all the complexes.

The sensitisation efficiencies calculated from the ratio  $Q_{\text{L}}^{\text{Eu}}/Q_{\text{Eu}}^{\text{Eu}}$  are close to unity for solid-state complexes, apart from the ones containing ligands with alkoxy groups (66–82%). In solution,  $\eta_{\text{sens}}$  values become smaller (77–83%), thereby resulting in lower overall quantum yields. The decrease of  $\eta_{\text{sens}}$  in solution can be explained by energy losses within the ligands both through collisional deactivation with solvent molecules and through their spatial re-arrangement with respect to the metal ion as a result of labile ligand-lanthanide binding (the latter may also be responsible for the broadening of the emission spectra in solution).

With respect to sensitisation of terbium luminescence in the solid state at room temperature, only the complex **TbL1** is emissive with  $Q_{\text{L}}^{\text{Tb}} = 9.0\%$  and  $\tau_{\text{obs}} = 0.3 \text{ ms}$  (Figure S17 in the Supporting Information), whereas **TbL4Me** is not. The triplet states of these ligands (20160 and 20410  $\text{cm}^{-1}$ , respectively, at 77 K) are close in energy to the  ${}^5\text{D}_4$  emissive level ( $\approx 20500 \text{ cm}^{-1}$ ), which probably results in Tb-to-ligand back energy transfer. On the other hand, both terbium complexes are emissive at 10 K with relatively long lifetimes: 1.45(1) ms for **TbL1** and 1.05(2) ms for **TbL4Me**. These two complexes represent an interesting study case since, despite

very similar  $E_T$  energy, they show very different luminescent properties at room temperature.

## Conclusion

Tridentate benzimidazole-substituted pyridine-2-carboxylates readily form 9-coordinate neutral homoleptic anhydrous lanthanide complexes and very efficiently sensitise the luminescence of europium, thereby leading to overall quantum yields as large as 71% in the solid state and 52% in  $\text{CH}_2\text{Cl}_2$ .

The photophysical properties of the europium complexes with ligands **L8R**<sup>-</sup> are not very sensitive to the nature of the substituent on the benzimidazole ring and remain essentially the same for R=H, F, Cl and Me. The heavy bromine atom redshifts the triplet energy of the ligand, which results in a large detrimental effect in solid-state samples. Other major changes are observed in the case of alkoxy groups, which significantly redshift absorption and triplet energy. As a result, the triplets in **EuL4O1** and **EuL8O8** are found to be only  $< 2050 \text{ cm}^{-1}$  above the  $^5\text{D}_0$  state, therefore allowing potential thermal back-energy transfer from europium to the ligand. However, a significant contribution of this deactivation pathway is unlikely since the observed lifetimes are almost temperature independent (Table S3 in the Supporting Information). On the other hand, temperature-independent energy losses in these two complexes may occur within ligands through the alkoxy-to-imine intra-benzimidazole charge-transfer state before energy transfer to the metal ion takes place. Whatever the exact mechanism is, its outcome is a lower sensitisation efficiency ( $\eta_{\text{sens}} < 82\%$ ). However, despite these energy losses, **EuL4O1** and **EuL8O8** display sizeable quantum yields in the range of 42–52%.

Figure 8 reveals that  $Q_L^{\text{Eu}}$  is approximately a monotonic function of the triplet-state energy in the investigated range and that quantum yields equal to or larger than 50% are obtained when  $E_T > 19300 \text{ cm}^{-1}$  for solid-state samples or  $E_T > 20300 \text{ cm}^{-1}$  for samples in  $\text{CH}_2\text{Cl}_2$ . This provides a guideline for the design of ligands suitable for the sensitisation of  $\text{Eu}^{\text{III}}$  luminescence. In the investigated systems, the ligand-to- $\text{Eu}^{\text{III}}$  energy transfer is almost quantitative in the solid state and approximately 80% in  $\text{CH}_2\text{Cl}_2$  for all of the complexes apart from **EuL8O8** and **EuL4O1**.

The remarkable photophysical properties of the europium complexes further result from the good protection of the metal ion by the ligands from non-radiative deactivation provided by the  $\text{N}_6\text{O}_3$  coordination environment. As a consequence, long and temperature-independent lifetimes are observed (2.4–3.0 ms). At the same time, the radiative lifetimes of  $\text{Eu}^{\text{III}}$  are relatively short (in the 3.6–4.6 ms range), which allows emissive processes to compete efficiently with non-radiative ones. As a comparison, a radiative lifetime of 9.7 ms is reported for the  $\text{Eu}^{\text{III}}$  aqua ion,<sup>[18]</sup> which would correspond to 6.8 ms in the solid state when applying the refractive index correction [1.5 vs. 1.333; see Eq. (4)]. The shorter lifetime implies more orbital mixing in the com-

plexes, probably due to the larger polarisability of N and O(carboxylate) atoms of the organic ligand compared to O(water) and the lower symmetry of the coordination environment ( $C_1$  for  $\text{N}_6\text{O}_3$  and  $D_{3h}$  for  $\text{O}_9$ ).

In conclusion, the described europium complexes with readily accessible benzimidazole-substituted pyridine-2-carboxylates are promising building blocks for the design of luminescent materials since they display large absorption, high luminescence efficiency, long luminescence lifetimes and adequate film-forming properties.

## Experimental Section

**General methods, equipment and chemicals used:** Elemental analyses were performed by Dr. E. Solari, Service for Elemental Analysis, Institute of Chemical and Chemical Engineering Sciences (EPFL).  $^1\text{H}$  NMR spectra were recorded using a Bruker Avance DRX 400 MHz spectrometer. Absorption spectra were measured using a Perkin–Elmer Lambda 900 UV/Vis/NIR spectrometer at room temperature in the spectral range 250–500 nm. Estimated errors are  $\pm 1 \text{ nm}$  for  $\lambda_{\text{max}}$  and  $\pm 5\%$  for  $\epsilon$ . Luminescence spectra were measured using a Fluorolog FL 3-22 spectrometer from Horiba–Jobin Yvon–Spex equipped for both visible and NIR measurements and were corrected for the instrumental function. Quantum yields were determined using the same instrument through an absolute method with a home-modified integrating sphere. Luminescence lifetimes were measured with a previously described instrumental setup.<sup>[32,36]</sup> Spectroscopic studies were conducted in optical cells of 2 mm path length or 2 mm i.d. quartz capillaries under air with the samples of lanthanide complexes obtained directly from the synthesis and used without further purification. The solutions of the complexes in  $\text{CH}_2\text{Cl}_2$  (Fisher Scientific, analytical reagent grade) were freshly prepared before each experiment. Thin films have been spin-coated from a solution of  $[\text{Eu}(\text{L8})_3]$  in  $\text{CH}_2\text{Cl}_2$  ( $2 \text{ mg mL}^{-1}$ ) on quartz substrates using a P-6708D spin-coater (Cookson Electronics). The rotation of substrate was 2000 rpm, and the solution volume was 1 mL. Their thickness has been estimated by profilometry to be approximately 50 nm.

**X-ray crystallography:** The crystal data and structure refinement parameters are presented in Table 6. To grow crystals for X-ray analysis, a small batch (1–2 mg) of the complex was dissolved in a small volume (1–3 mL) of boiling  $\text{CH}_3\text{CN}$  in the case of **EuL4Me** and **LnL4O1** (La, Eu), or  $\text{CH}_3\text{CN}/\text{CH}_3\text{OH}$  for others. This was followed by cooling and slow evaporation of the solution for 1–4 weeks under air in the dark.

Data collection for the eight crystal structures was performed at low temperature using  $\text{MoK}\alpha$  radiation. An Oxford Diffraction Sapphire/KM4 CCD was employed for **EuL1**, **EuL4O1** and **LnL4Me** (La, Eu), whereas the remaining samples were measured using a Bruker APEX II CCD. Both diffractometers have a kappa geometry goniometer. Data were reduced by means of CrysAlis PRO<sup>[47]</sup> for **EuL1**, **EuL4O1** and **LnL4Me** (La, Eu) or EvalCCD<sup>[48]</sup> for others and then corrected for absorption.<sup>[49]</sup> Solution and refinement for all crystal structures were performed by using SHELX.<sup>[50]</sup> All structures were refined using full-matrix least-squares on  $F^2$  with all non-hydrogen atoms anisotropically defined. Hydrogen atoms were placed in calculated positions by means of the “riding” model.

The following disorder problems have been encountered during the last stages of refinement. 1) For **LnL4O1** (La, Eu), two  $\text{CH}_3\text{CN}$  were highly disordered and their disorder dealt also with the presence of  $0.5\text{H}_2\text{O}$ . They have been treated by the split model and then some constraints (equal anisotropic displacement parameters (EADP) command in SHELX)<sup>[50]</sup> applied in the case of **EuL4O1**. 2) In the case of **EuL4Me**, an alkyl chain (C14, ..., C17) was disordered and a split model with some restraints (SADI, SIMU)<sup>[50]</sup> was applied to treat it. 3) The very low quality and weakness of the measured diffraction for **LaL4Me** prevented us from treating the solvent as was done for **TbL4Me**. The SQUEEZE routine in-

Table 6. Crystal data and structure refinement.<sup>[a]</sup>

|   | [La(L1) <sub>3</sub> ]  | [Eu(L1) <sub>3</sub> ]   | [Tb(L1) <sub>3</sub> ]   | [La(L4Me) <sub>3</sub> ]   |
|---|---|--|--|--|
| formula   | C <sub>42</sub> H <sub>30</sub> LaN <sub>9</sub> O <sub>6</sub> ·CH <sub>3</sub> CN       | C <sub>42</sub> H <sub>30</sub> EuN <sub>9</sub> O <sub>6</sub> ·CH <sub>3</sub> CN                            | C <sub>42</sub> H <sub>30</sub> N <sub>9</sub> O <sub>6</sub> Tb·2.5 CH <sub>3</sub> CN                        | C <sub>54</sub> H <sub>54</sub> LaN <sub>9</sub> O <sub>6</sub>  |
| <i>M<sub>r</sub></i>                                | 936.71  | 949.76   | 1018.30  | 1063.97  |
| <i>T</i> [K]  | 100(2)  | 140(2)   | 100(2)   | 140(2)   |
| crystal system                                      | monoclinic  | monoclinic   | triclinic  | monoclinic   |
| space group   | <i>P</i> 2 <sub>1</sub> / <i>c</i>  | <i>P</i> 2 <sub>1</sub> / <i>c</i>   | <i>P</i> 1̄  | <i>P</i> 2 <sub>1</sub> / <i>c</i>   |
| <i>a</i> [Å]  | 11.3182(15)   | 11.2030(4)   | 11.0872(14)  | 21.8689(17)  |
| <i>b</i> [Å]  | 24.856(2)   | 24.5654(8)   | 11.2398(17)  | 20.4015(12)  |
| <i>c</i> [Å]  | 14.053(2)   | 14.0980(5)   | 18.0694(15)  | 25.951(2)  |
| <i>α</i> [°]  | 90  | 90   | 78.929(9)  | 90   |
| <i>β</i> [°]  | 100.331(10)   | 100.659(3)   | 74.700(8)  | 111.986(9)   |
| <i>γ</i> [°]  | 90  | 90   | 85.722(10)   | 90   |
| <i>V</i> [Å <sup>3</sup> ]                          | 3889.4(8)   | 3812.9(2)  | 2130.9(5)  | 10736.3(14)  |
| <i>Z</i>  | 4   | 4  | 2  | 8  |
| <i>ρ</i> <sub>calcd</sub> [Mg m <sup>-3</sup> ]     | 1.600   | 1.655  | 1.587  | 1.316  |
| <i>μ</i> [mm <sup>-1</sup> ]                        | 1.164   | 1.712  | 1.726  | 0.851  |
| <i>F</i> (000)                                      | 1888  | 1912   | 1026   | 4368   |
| crystal size [mm <sup>3</sup> ]                     | 0.36 × 0.23 × 0.19  | 0.40 × 0.32 × 0.22   | 0.34 × 0.26 × 0.14   | 0.10 × 0.08 × 0.06   |
| <i>θ</i> range [°]                                  | 3.37–27.51  | 2.70–26.37   | 3.40–27.50   | 2.57–25.03   |
| index ranges  | −14 ≤ <i>h</i> ≤ 14<br>−32 ≤ <i>k</i> ≤ 31<br>−18 ≤ <i>l</i> ≤ 18                         | −4 ≤ <i>h</i> ≤ 14<br>−30 ≤ <i>k</i> ≤ 17<br>−17 ≤ <i>l</i> ≤ 17   | −14 ≤ <i>h</i> ≤ 14<br>−14 ≤ <i>k</i> ≤ 14<br>−23 ≤ <i>l</i> ≤ 23  | −26 ≤ <i>h</i> ≤ 23<br>−24 ≤ <i>k</i> ≤ 24<br>−30 ≤ <i>l</i> ≤ 30  |
| reflns collected                                    | 85 674  | 28 347   | 42 605   | 86 741   |
| independent reflns                                  | 8927 ( <i>R</i> <sub>int</sub> = 0.0715)  | 7752 ( <i>R</i> <sub>int</sub> = 0.0672)   | 9645 ( <i>R</i> <sub>int</sub> = 0.0518)   | 18 927 ( <i>R</i> <sub>int</sub> = 0.2666)   |
| completeness to <i>θ</i> [°] [%]                    | 27.51 (99.7)  | 26.37 (99.5)   | 27.50 (98.4)   | 25.03 (99.8)   |
| max/min transm                                      | 0.802/0.677   | 0.686/0.659  | 0.785/0.552  | 0.950/0.816  |
| data/restraints/params                              | 8927/0/550  | 7752/0/550   | 9645/18/676  | 18 927/900/1177  |
| GOF on <i>F</i> <sup>2</sup>                        | 1.345   | 0.911  | 1.165  | 0.911  |
| final <i>R</i> indices ( <i>I</i> > 2σ( <i>I</i> )) | <i>R</i> 1 = 0.0534, <i>wR</i> 2 = 0.1456   | <i>R</i> 1 = 0.0360, <i>wR</i> 2 = 0.0569  | <i>R</i> 1 = 0.0392, <i>wR</i> 2 = 0.0962  | <i>R</i> 1 = 0.1127, <i>wR</i> 2 = 0.2190  |
| <i>R</i> indices (all data)                         | <i>R</i> 1 = 0.0653, <i>wR</i> 2 = 0.1496   | <i>R</i> 1 = 0.0703, <i>wR</i> 2 = 0.0618  | <i>R</i> 1 = 0.0491, <i>wR</i> 2 = 0.1022  | <i>R</i> 1 = 0.2711, <i>wR</i> 2 = 0.2752  |
| largest diff. peak/hole [e Å <sup>-3</sup> ]        | 1.870/−1.352  | 0.725/−0.769   | 1.867/−1.137   | 3.488/−2.676   |
|   | [Eu(L4Me) <sub>3</sub> ]  | [Tb(L4Me) <sub>3</sub> ]   | [La(L4O1) <sub>3</sub> ]   | [Eu(L4O1) <sub>3</sub> ]   |
| formula   | C <sub>54</sub> H <sub>54</sub> EuN <sub>9</sub> O <sub>6</sub> ·<br>2 CH <sub>3</sub> CN | 2 C <sub>54</sub> H <sub>54</sub> N <sub>9</sub> O <sub>6</sub> Tb·<br>3 CH <sub>3</sub> CN·4 H <sub>2</sub> O | C <sub>54</sub> H <sub>54</sub> LaN <sub>9</sub> O <sub>6</sub> ·<br>3 CH <sub>3</sub> CN·0.5 H <sub>2</sub> O | C <sub>54</sub> H <sub>54</sub> EuN <sub>9</sub> O <sub>6</sub> ·<br>3 CH <sub>3</sub> CN·0.5 H <sub>2</sub> O |
| <i>M<sub>r</sub></i>                                | 1159.13   | 2363.19  | 1244.14  | 1257.19  |
| <i>T</i> [K]  | 140(2)  | 100(2)   | 100(2)   | 140(2)   |
| crystal system                                      | monoclinic  | monoclinic   | triclinic  | triclinic  |
| space group   | <i>P</i> 2 <sub>1</sub> / <i>n</i>  | <i>P</i> 2 <sub>1</sub> / <i>c</i>   | <i>P</i> 1̄  | <i>P</i> 1̄  |
| <i>a</i> [Å]  | 12.5508(3)  | 22.013(3)  | 12.7553(11)  | 12.5901(7)   |
| <i>b</i> [Å]  | 19.3849(4)  | 20.350(3)  | 15.0195(16)  | 14.9590(10)  |
| <i>c</i> [Å]  | 22.5701(6)  | 25.934(4)  | 16.1388(18)  | 16.1459(10)  |
| <i>α</i> [°]  | 90  | 90   | 78.899(8)  | 78.632(5)  |
| <i>β</i> [°]  | 104.173(3)  | 112.221(7)   | 73.727(9)  | 73.446(5)  |
| <i>γ</i> [°]  | 90  | 90   | 77.393(8)  | 77.922(5)  |
| <i>V</i> [Å <sup>3</sup> ]                          | 5324.1(2)   | 10755(3)   | 2867.8(5)  | 2819.4(3)  |
| <i>Z</i>  | 4   | 4  | 2  | 2  |
| <i>ρ</i> <sub>calcd</sub> [Mg m <sup>-3</sup> ]     | 1.446   | 1.459  | 1.441  | 1.481  |
| <i>μ</i> [mm <sup>-1</sup> ]                        | 1.241   | 1.381  | 0.814  | 1.183  |
| <i>F</i> (000)                                      | 2384  | 4856   | 1282   | 1294   |
| crystal size [mm <sup>3</sup> ]                     | 0.45 × 0.39 × 0.25  | 0.51 × 0.31 × 0.23   | 0.51 × 0.16 × 0.12   | 0.32 × 0.30 × 0.25   |
| <i>θ</i> range [°]                                  | 2.69–26.37  | 3.31–27.51   | 3.31–27.50   | 2.62–26.02   |
| index ranges  | −15 ≤ <i>h</i> ≤ 15<br>−21 ≤ <i>k</i> ≤ 24<br>−28 ≤ <i>l</i> ≤ 28                         | −28 ≤ <i>h</i> ≤ 28<br>−26 ≤ <i>k</i> ≤ 26<br>−33 ≤ <i>l</i> ≤ 33  | −16 ≤ <i>h</i> ≤ 16<br>−19 ≤ <i>k</i> ≤ 19<br>−20 ≤ <i>l</i> ≤ 20  | −15 ≤ <i>h</i> ≤ 15<br>−17 ≤ <i>k</i> ≤ 18<br>−18 ≤ <i>l</i> ≤ 19  |
| reflns collected                                    | 41 483  | 25 8860  | 70 501   | 21 213   |
| independent reflns                                  | 10 815 ( <i>R</i> (int) = 0.0730)   | 24 631 ( <i>R</i> (int) = 0.0629)  | 13 137 ( <i>R</i> (int) = 0.0569)  | 11 062 ( <i>R</i> (int) = 0.1069)  |
| completeness to <i>θ</i> [°] [%]                    | 26.37 (99.3)  | 27.51 (99.6)   | 27.50 (99.6)   | 26.02 (99.4)   |
| max/min transm                                      | 1.0000/0.88680  | 0.728/0.540  | 1.0000/0.7964  | 0.744/0.663  |
| data/restraints/params                              | 10 815/27/713   | 24 631/0/1378  | 13 137/3/808   | 11 062/9/773   |
| GOF on <i>F</i> <sup>2</sup>                        | 0.886   | 1.140  | 1.130  | 0.798  |
| final <i>R</i> indices ( <i>I</i> > 2σ( <i>I</i> )) | <i>R</i> 1 = 0.0389, <i>wR</i> 2 = 0.0617   | <i>R</i> 1 = 0.0471, <i>wR</i> 2 = 0.0982  | <i>R</i> 1 = 0.0370, <i>wR</i> 2 = 0.0628  | <i>R</i> 1 = 0.0635, <i>wR</i> 2 = 0.0559  |
| <i>R</i> indices (all data)                         | <i>R</i> 1 = 0.0899, <i>wR</i> 2 = 0.0698   | <i>R</i> 1 = 0.0713, <i>wR</i> 2 = 0.1119  | <i>R</i> 1 = 0.0531, <i>wR</i> 2 = 0.0681  | <i>R</i> 1 = 0.1446, <i>wR</i> 2 = 0.0668  |
| largest diff. peak/hole [e Å <sup>-3</sup> ]        | 0.770/−0.512  | 2.935/−2.669   | 0.483/−0.484   | 1.147/−0.984   |

[a] Data in common:  $\lambda = 0.71073$  Å; refinement method: full-matrix least-squares on *F*<sup>2</sup>; absorption correction: semi-empirical from equivalents.

cluded within PLATON<sup>[51]</sup> was then used to treat the unresolved solvent. The anisotropic refinement of the light atoms (C, N and O) was very difficult as well and some restraints were applied to their displacement parameters. 4) One of the ligands in **TbL1** showed two slightly different orientations. The split model perfectly solved this kind of disorder that dealt also with the presence of 0.5 CH<sub>3</sub>CN, very close to the *N*-methylbenzimidazole moiety of the ligand. Additional constraints (SIMU) were applied to the displacement parameters of the above-mentioned disordered ligand.

**General synthesis of benzimidazole-substituted pyridine-2-carboxylic acids:** The synthesis of the precursors is described in the Supporting Information. The reactions were performed under air. Substituted pyridine-2-carboxaldehyde was dissolved in formic acid (Merck, 98–100%) at RT to give a yellow solution that sometimes appeared as being cloudy due to the presence of a red solid, which was probably residual Se from the previous synthetic step. The amount of formic acid was chosen to correspond either to a minimum of 3–5 molar equivalents relative to aldehyde or to the minimum volume necessary to dissolve the aldehyde at 0°C. This solution was cooled to 0°C, stirred for 10 min and cold H<sub>2</sub>O<sub>2</sub> (30 wt% aq solution) was added in excess. The solution was stirred and occasionally briefly sonicated at 0°C for 4–6 h, and kept overnight at 0°C. Addition of ice-cold water (20 mL) precipitated the product. The resulting suspension was stirred at 0°C for 1 h and filtered to give a white solid. It was washed with water, hexane and a small amount of hexane/ether (1:1) for **HL401** or water and hexane in all other cases and was dried under vacuum. Further synthetic details are provided below.

**Synthesis of HL401:** The reaction was performed with **L401-CHO** (555 mg, 1.79 mmol), formic acid (3 mL, 3.66 g, 0.08 mol) and H<sub>2</sub>O<sub>2</sub> (1.05 mL of 30 wt% aq solution, contains 350 mg of H<sub>2</sub>O<sub>2</sub>, 10.3 mmol). Addition of water did not result in precipitation of the product. Therefore, aqueous NaHCO<sub>3</sub> was added dropwise to this solution until pH 2. The resulting suspension was stirred at 0°C for 2 h and filtered, and the solid was treated as described in the general procedure. White solid: 462 mg (1.35 mmol, 75%). <sup>1</sup>H NMR (400 MHz, [D<sub>6</sub>]DMSO): δ = 8.47 (dd, *J* = 6.4, 1.2 Hz, 1H), 8.16–8.05 (m, 2H), 7.62 (d, *J* = 8.8 Hz, 1H), 7.19 (d, *J* = 2.4 Hz, 1H), 6.90 (dd, *J* = 8.8, 2.4 Hz, 1H), 4.90 (t, *J* = 7.2 Hz, 2H), 3.87 (s, 3H), 1.78 (p, *J* = 7.6 Hz, 2H), 1.34 (sextet, *J* = 7.6 Hz, 2H), 0.85 ppm (t, *J* = 7.2 Hz, 3H); CO<sub>2</sub>H proton was not observed; elemental analysis calcd (%) for C<sub>18</sub>H<sub>19</sub>N<sub>3</sub>O<sub>3</sub>·H<sub>2</sub>O (343.38): C 62.96, H 6.16, N 12.24; found: C 62.98, H 6.11, N 12.15.

**Synthesis of HL8:** The reaction was performed with **L8-CHO** (446 mg, 1.33 mmol), formic acid (5 mL, 6.1 g, 0.13 mol) and H<sub>2</sub>O<sub>2</sub> (0.75 mL of 30 wt% aq solution, containing 250 mg of H<sub>2</sub>O<sub>2</sub>, 7.34 mmol). White solid: 410 mg (1.17 mmol, 88%). <sup>1</sup>H NMR (400 MHz, [D<sub>6</sub>]DMSO): δ = 8.51 (d, *J* = 7.2 Hz, 1H), 8.21–8.07 (m, 2H), 7.74 (d, *J* = 8.0 Hz, 1H), 7.68 (d, *J* = 8.0 Hz, 1H), 7.34 (t, *J* = 7.2 Hz, 1H), 7.28 (t, *J* = 7.2 Hz, 1H), 4.94 (t, *J* = 7.6 Hz, 2H), 1.79 (p, *J* = 7.2 Hz, 2H), 1.35–1.10 (m, 10H), 0.81 ppm (t, *J* = 6.8 Hz, 3H); CO<sub>2</sub>H proton was not observed; elemental analysis calcd (%) for C<sub>21</sub>H<sub>25</sub>N<sub>3</sub>O<sub>2</sub> (351.44): C 71.77, H 7.17, N 11.96; found: C 71.82, H 7.08, N 11.94.

**Synthesis of HL8F:** The reaction was performed with **L8F-CHO** (501 mg, 1.42 mmol), formic acid (5 mL, 6.1 g, 0.13 mol) and H<sub>2</sub>O<sub>2</sub> (0.8 mL of 30 wt% aq solution, containing 266 mg of H<sub>2</sub>O<sub>2</sub>, 7.83 mmol). White solid: 471 mg (1.27 mmol, 90%). <sup>1</sup>H NMR (400 MHz, [D<sub>6</sub>]DMSO): δ = 8.49 (d, *J* = 6.4 Hz, 1H), 8.20–8.09 (m, 2H), 7.75 (dd, *J* = 8.8, 5.2 Hz, 1H), 7.62 (dd, *J* = 10, 2.4 Hz, 1H), 7.14 (td, *J* = 9.6, 2.4 Hz, 1H), 4.90 (t, *J* = 7.2 Hz, 2H), 1.81–1.70 (brp, 2H), 1.35–1.09 (m, 10H), 0.81 ppm (t, *J* = 7.2 Hz, 3H); CO<sub>2</sub>H proton was not observed; elemental analysis calcd (%) for C<sub>21</sub>H<sub>24</sub>FN<sub>3</sub>O<sub>2</sub> (369.43): C 68.27, H 6.55, N 11.37; found: C 68.47, H 6.58, N 11.38.

**Synthesis of HL8Cl:** The reaction was performed with **L8Cl-CHO** (484 mg, 1.31 mmol), formic acid (5 mL, 6.1 g, 0.13 mol) and H<sub>2</sub>O<sub>2</sub> (0.7 mL of 30 wt% aq solution, containing 233 mg of H<sub>2</sub>O<sub>2</sub>, 6.85 mmol). White solid: 466 mg (1.21 mmol, 92%). <sup>1</sup>H NMR (400 MHz, [D<sub>6</sub>]DMSO): δ = 8.50 (d, *J* = 6.4 Hz, 1H), 8.22–8.11 (m, 2H), 7.87 (d, *J* = 1.6 Hz, 1H), 7.75 (d, *J* = 8.8 Hz, 1H), 7.30 (dd, *J* = 8.4, 1.6 Hz, 1H), 4.93 (t, *J* = 7.2 Hz, 2H), 1.81–1.70 (brp, 2H), 1.35–1.09 (m, 10H), 0.81 ppm (t, *J* = 7.2 Hz, 3H); CO<sub>2</sub>H proton was not observed; elemental analysis calcd

(%) for C<sub>21</sub>H<sub>24</sub>ClN<sub>3</sub>O<sub>2</sub> (385.89): C 65.36, H 6.27, N 10.89; found: C 65.36, H 6.28, N 10.71.

**Synthesis of HL8Br:** The reaction was performed with **L8Br-CHO** (564 mg, 1.36 mmol), formic acid (4 mL, 4.9 g, 0.10 mol) and H<sub>2</sub>O<sub>2</sub> (0.7 mL of 30 wt% aq solution, containing 233 mg of H<sub>2</sub>O<sub>2</sub>, 6.85 mmol). White solid: 503 mg (1.17 mmol, 86%). <sup>1</sup>H NMR (400 MHz, [D<sub>6</sub>]DMSO): δ = 8.51 (dd, *J* = 7.2, 2.0 Hz, 1H), 8.21–8.12 (m, 2H), 8.01 (d, *J* = 1.2 Hz, 1H), 7.70 (d, *J* = 8.8 Hz, 1H), 7.42 (dd, *J* = 8.4, 1.6 Hz, 1H), 4.93 (t, *J* = 7.2 Hz, 2H), 1.8–1.7 (brm, 2H), 1.34–1.08 (brm, 10H), 0.81 ppm (t, *J* = 7.2 Hz, 3H); CO<sub>2</sub>H proton was not observed; elemental analysis calcd (%) for C<sub>21</sub>H<sub>24</sub>BrN<sub>3</sub>O<sub>2</sub> (430.34): C 58.61, H 5.62, N 9.76; found: C 58.96, H 5.67, N 9.68.

**Synthesis of HL8Me:** The reaction was performed with **L8Me-CHO** (583 mg, 1.66 mmol), formic acid (4 mL, 4.9 g, 0.11 mol) and H<sub>2</sub>O<sub>2</sub> (0.85 mL of 30 wt% aq solution, containing 283 mg of H<sub>2</sub>O<sub>2</sub>, 8.32 mmol). White solid: 568 mg (1.45 mmol, 87%). <sup>1</sup>H NMR (400 MHz, [D<sub>6</sub>]acetone): δ = 8.63 (dd, *J* = 6.8, 1.6 Hz, 1H), 8.23–8.14 (m, 2H), 8.12 (s, 0.5H; HCO<sub>2</sub>H), 7.61 (d, *J* = 8.0 Hz, 1H), 7.45 (s, 1H), 7.13 (d, *J* = 8.0 Hz, 1H), 4.96 (t, *J* = 7.6 Hz, 2H), 2.51 (s, 3H), 2.0–1.85 (m, 2H), 1.48–1.17 (m, 10H), 0.84 ppm (t, *J* = 6.8 Hz, 3H); CO<sub>2</sub>H proton not observed; the presence of HCO<sub>2</sub>H has been confirmed and quantified by <sup>1</sup>H NMR in [D<sub>6</sub>]acetone: δ = 8.12 ppm (s); elemental analysis calcd (%) for C<sub>22</sub>H<sub>27</sub>N<sub>3</sub>O<sub>2</sub>·0.5HCO<sub>2</sub>H·0.25H<sub>2</sub>O (392.99): C 68.77, H 7.31, N 10.69; found: C 68.76, H 7.36, N 10.72.

**Synthesis of HL8O8:** The reaction was performed with **L8O8-CHO** (732 mg, 1.58 mmol), formic acid (5 mL, 6.1 g, 0.13 mol) and H<sub>2</sub>O<sub>2</sub> (0.81 mL of 30 wt% aq solution, containing 270 mg of H<sub>2</sub>O<sub>2</sub>, 7.93 mmol). The product separates as sticky pink oil that solidifies on stirring and sonication. Pale pink solid: 601 mg (1.25 mmol, 79%). <sup>1</sup>H NMR (400 MHz, [D<sub>6</sub>]DMSO): δ = 8.45 (dd, *J* = 7.6, 1.2 Hz, 1H), 8.15–8.05 (m, 2H), 7.60 (d, *J* = 8.8 Hz, 1H), 7.16 (d, *J* = 2.0 Hz, 1H), 6.89 (dd, *J* = 8.8, 2.0 Hz, 1H), 4.90 (t, *J* = 7.2 Hz, 2H), 4.06 (t, *J* = 6.8 Hz, 2H), 1.81–1.69 (m, 4H), 1.5–1.4 (m, 2H) 1.4–1.1 (m, 18H), 0.87 (t, *J* = 6.8 Hz, 3H), 0.81 ppm (t, *J* = 7.2 Hz, 3H); CO<sub>2</sub>H proton not observed; elemental analysis calcd (%) for C<sub>20</sub>H<sub>41</sub>N<sub>3</sub>O<sub>3</sub> (479.65): C 72.62, H 8.62, N 8.76; found: C 72.23, H 8.85, N 8.74.

**Synthesis of lanthanide complexes:** The reactions were performed under air using a 3:3:1 molar ratio of the ligand, NaOH and LnCl<sub>3</sub>·*n*H<sub>2</sub>O. The ligand was suspended in hot ethanol (70–80°C, 5 mL); the same temperature was kept throughout the reaction, followed by addition of NaOH dissolved in water (0.5–1 mL, used as a stock solution with approx. 100 mg of NaOH per 10 mL of water) and stirring for 10 min to give colourless solution. A solution of LnCl<sub>3</sub>·*n*H<sub>2</sub>O (*n* = 6 or 7; 99.9%, Aldrich) in water (2 mL) was added dropwise over 5 min and stirred for a further 5 min. A white precipitate of the complex may form on addition. An additional volume of water (specified below) was added to complete precipitation of the complex. The resulting suspension was stirred for 10 min at 70–80°C, cooled to 40–50°C and filtered while warm. The product was washed with ethanol/water (1:1) followed by ether for **LnL1**, **LnL4Me** and **LnL401** or with ethanol/water (1:1) followed by hexane in all other cases and was dried under vacuum at room temperature. The complexes are white solids that are soluble in DMSO, boiling ethanol and are insoluble in hexane and water; the complexes with *N*-octyl groups are also soluble in CH<sub>2</sub>Cl<sub>2</sub>. <sup>1</sup>H NMR spectroscopy of the diamagnetic lanthanum complexes in CD<sub>2</sub>Cl<sub>2</sub> at 10<sup>−3</sup> M was not informative, as all resonances were very broad at room temperature. Further synthetic details and analytical data for Eu complexes are provided below, whereas data for the La and Tb complexes are given in the Supporting Information.

**Synthesis of [Eu(L8)<sub>3</sub>]:** The complex was precipitated with water (5 mL). Yield: 45 mg (0.037 mmol, 80%) from **HL8** (50 mg, 0.142 mmol), NaOH (5.69 mg, 0.142 mmol) and EuCl<sub>3</sub>·6H<sub>2</sub>O (17.4 mg, 0.047 mmol); elemental analysis calcd (%) for C<sub>63</sub>H<sub>72</sub>EuN<sub>9</sub>O<sub>6</sub> (1203.27): C 62.88, H 6.03, N 10.48; found: C 63.03, H 6.08, N 10.27.

**Synthesis of [Eu(L8F)<sub>3</sub>]:** The complex was precipitated with water (2 mL). Yield: 50 mg (0.040 mmol, 88%) from **HL8F** (50 mg, 0.135 mmol), NaOH (5.41 mg, 0.135 mmol) and EuCl<sub>3</sub>·6H<sub>2</sub>O (16.5 mg, 0.045 mmol); elemental analysis calcd (%) for C<sub>63</sub>H<sub>69</sub>EuF<sub>3</sub>N<sub>9</sub>O<sub>6</sub> (1257.24): C 60.19, H 5.53; N 10.03; found: C 60.32, H 5.53, N 10.04.

**Synthesis of [Eu(L8Cl)<sub>3</sub>]:** The complex was precipitated with water (2 mL). Yield: 43 mg (0.033 mmol, 77 %) from **HL8Cl** (50 mg, 0.130 mmol), NaOH (5.18 mg, 0.130 mmol) and EuCl<sub>3</sub>·6H<sub>2</sub>O (15.8 mg, 0.043 mmol); elemental analysis calcd (%) for C<sub>63</sub>H<sub>69</sub>Cl<sub>3</sub>EuN<sub>9</sub>O<sub>6</sub> (1306.60): C 57.91, H 5.32, N 9.65; found: C 58.03, H 5.32, N 9.52.

**Synthesis of [Eu(L8Br)<sub>3</sub>]:** The complex was precipitated with water (2 mL). Yield: 42 mg (0.029 mmol, 75 %) from **HL8Br** (50 mg, 0.116 mmol), NaOH (4.65 mg, 0.116 mmol) and EuCl<sub>3</sub>·6H<sub>2</sub>O (14.2 mg, 0.039 mmol); elemental analysis calcd (%) for C<sub>63</sub>H<sub>73</sub>Br<sub>3</sub>EuN<sub>9</sub>O<sub>8</sub> (1439.95): C 52.55, H 4.83, N 8.75; found: C 52.66, H 4.87, N 8.68.

**Synthesis of [Eu(L8Me)<sub>3</sub>]-0.5H<sub>2</sub>O:** The complex was precipitated with water (5 mL). Yield: 38 mg (0.030 mmol, 72 %) from **HL8Me** (50 mg, 0.127 mmol), NaOH (5.09 mg, 0.127 mmol) and EuCl<sub>3</sub>·6H<sub>2</sub>O (15.54 mg, 0.042 mmol); elemental analysis calcd (%) for C<sub>66</sub>H<sub>78</sub>EuN<sub>9</sub>O<sub>6</sub>·0.5H<sub>2</sub>O (1254.35): C 63.20, H 6.35, N 10.05; found: C 63.14, H 6.39, N 9.87.

**Synthesis of [Eu(L8O8)<sub>3</sub>]-1.5H<sub>2</sub>O:** The complex was precipitated with water (1 mL). Yield: 40 mg (0.025 mmol, 71 %) from **HL8O8** (50 mg, 0.104 mmol), NaOH (4.17 mg, 0.104 mmol) and EuCl<sub>3</sub>·6H<sub>2</sub>O (12.73 mg, 0.035 mmol); elemental analysis calcd (%) for C<sub>87</sub>H<sub>120</sub>EuN<sub>9</sub>O<sub>9</sub>·1.5H<sub>2</sub>O (1614.93): C 64.70, H 7.68, N 7.81; found: C 64.72, H 7.69, N 7.71.

**Synthesis of [Eu(L4O1)<sub>3</sub>]-H<sub>2</sub>O:** The complex was precipitated with water (2 mL). Yield: 45 mg (0.039 mmol, 82 %) from **HL4O1-H<sub>2</sub>O** (50 mg, 0.146 mmol), NaOH (5.82 mg, 0.146 mmol) and EuCl<sub>3</sub>·6H<sub>2</sub>O (17.7 mg, 0.048 mmol); elemental analysis calcd (%) for C<sub>54</sub>H<sub>54</sub>EuN<sub>9</sub>O<sub>9</sub>·H<sub>2</sub>O (1143.04): C 56.74, H 4.94, N 11.03; found: C 56.49, H 4.93, N 10.90.

**Crystallographic data:** CCDC-736923 [La(L1)<sub>3</sub>], 736925 [Tb(L1)<sub>3</sub>], 736926 [La(L4Me)<sub>3</sub>], 736927 [Eu(L4Me)<sub>3</sub>], 736928 [Tb(L4Me)<sub>3</sub>], 736929 [La(L4O1)<sub>3</sub>] and 736930 [Eu(L4O1)<sub>3</sub>] contain the supplementary crystallographic data for this paper. These data can be obtained free of charge from The Cambridge Crystallographic Data Centre via [www.ccdc.cam.ac.uk/data\\_request/cif](http://www.ccdc.cam.ac.uk/data_request/cif).

## Acknowledgements

This research is supported by a grant from the Swiss National Science Foundation (grant no. 20020 119866). We would like to acknowledge Frédéric Gumy (EPFL) for performing photophysical measurements on [Eu(L4O1)<sub>3</sub>]-H<sub>2</sub>O and Dr. Rosendo Sanjines (EPFL) for measuring the thickness of the thin films. JCB thanks the WCU (World Class University) program from the National Science Foundation of Korea (Ministry of Education, Science, and Technology) for grant R31-10035.

- [1] A. E. Demarçais, *C. R. Acad. Sci. Paris* **1901**, 132, 1484–1486.
- [2] R. M. Supkowski, W. D. Horrocks Jr., *Inorg. Chim. Acta* **2002**, 340, 44–48.
- [3] A. Beeby, I. M. Clarkson, R. S. Dickins, S. Faulkner, D. Parker, L. Royle, A. S. de Sousa, J. A. G. Williams, M. Woods, *J. Chem. Soc. Perkin Trans. 2* **1999**, 493–503.
- [4] J.-C. G. Bünzli, S. Petoud, E. Moret, *Spectrosc. Lett.* **1999**, 32, 155–163.
- [5] D. Ananias, M. Kostova, F. A. A. Paz, A. N. C. Neto, R. T. De Moura, O. L. Malta, L. D. Carlos, J. Rocha, *J. Am. Chem. Soc.* **2009**, 131, 8620–8626.
- [6] J.-C. G. Bünzli in *Lanthanide Probes in Life, Chemical and Earth Sciences. Theory and Practice* (Eds.: J.-C. G. Bünzli, G. R. Choppin), Elsevier, Amsterdam, **1989**, Chapter 7, pp. 219–293.
- [7] “Rationalization of crystal field parameterization”: C. Görlner-Walrand, K. Binnemans in *Handbook on the Physics and Chemistry of Rare Earths, Vol. 23* (Eds.: K. A. Gschneidner, Jr., L. Eyring), Elsevier, Amsterdam, **1996**, Chapter 155, pp. 121–283.
- [8] T. Jüstel, H. Nikol, C. Ronda, *Angew. Chem. Int. Ed.* **1998**, 110, 3250–3271; *Angew. Chem. Int. Ed.* **1998**, 37, 3084–3103.
- [9] G. Urbain, *Chem. Rev.* **1924**, 1, 143–185.
- [10] J.-C. G. Bünzli, C. Piguet, *Chem. Soc. Rev.* **2005**, 34, 1048–1077.

- [11] S. V. Eliseeva, J.-C. G. Bünzli, *Chem. Soc. Rev.* **2009**, DOI: 10.1039/b905604c.
- [12] A. de Bettencourt-Dias, *Dalton Trans.* **2007**, 2229–2241.
- [13] D. F. Reardon, US Patent 2008305243A1 20081211, **2008**.
- [14] S. Lian, C. Rong, D. Yin, S. Liu, *J. Phys. Chem. C* **2009**, 113, 6298–6302.
- [15] T. Gunnlaugsson, G. A. Leonard, *Chem. Commun.* **2005**, 3114–3131.
- [16] I. Hemmilä, V. Laitala, *J. Fluoresc.* **2005**, 15, 529–542.
- [17] J.-C. G. Bünzli, *Chem. Lett.* **2009**, 38, 104–109.
- [18] “The Absorption and Fluorescence Spectra of Rare Earth Ions in Solution”: W. T. Carnall in *Handbook on the Physics and Chemistry of Rare Earths, Vol. 3* (Eds.: K. A. Gschneidner, Jr., L. Eyring), North Holland, Amsterdam, **1979**, Chapter 24, pp. 172–208.
- [19] G. F. de Sá, O. L. Malta, C. D. Donega, A. M. Simas, R. L. Longo, P. A. Santa-Cruz, E. F. da Silva, *Coord. Chem. Rev.* **2000**, 196, 165–195.
- [20] N. M. Shavaleev, R. Scopelliti, F. Gumy, J.-C. G. Bünzli, *Inorg. Chem.* **2009**, 48, 5611–5613.
- [21] G. D. R. Napier, J. D. Neilson, T. M. Sheperd, *Chem. Phys. Lett.* **1975**, 31, 328–330.
- [22] L. N. Puntus, K. A. Lyssenko, I. Pekareva, J.-C. G. Bünzli, *J. Phys. Chem. B* **2009**, 113, 9265–9277.
- [23] S. Sato, M. Wada, *Bull. Chem. Soc. Jpn.* **1970**, 43, 1955–1962.
- [24] “Rare Earth β-Diketonate Complexes: Functionalities and Applications”: K. Binnemans in *Handbook on the Physics and Chemistry of Rare Earths, Vol. 35* (Eds.: K. A. Gschneidner, Jr., J.-C. G. Bünzli, V. K. Pecharsky), Elsevier, Amsterdam, **2005**, Chapter 225, pp. 107–272.
- [25] R. Ziessel, S. Diring, P. Kadjane, L. J. Charbonnière, P. Retailleau, C. Philouze, *Chem. Asian J.* **2007**, 2, 975–982.
- [26] C. R. De Silva, J. R. Maeyer, A. Dawson, Z. P. Zheng, *Polyhedron* **2007**, 26, 1229–1238.
- [27] K. Nakamura, Y. Hasegawa, H. Kawai, N. Yasuda, N. Kanehisa, Y. Kai, T. Nagamura, S. Yanagida, Y. Wada, *J. Phys. Chem. A* **2007**, 111, 3029–3037.
- [28] C. Yang, L. M. Fu, Y. Wang, J. P. Zhang, W. T. Wong, X. C. Ai, Y. F. Qiao, B. S. Zou, L. L. Gui, *Angew. Chem.* **2004**, 116, 5120–5123; *Angew. Chem. Int. Ed.* **2004**, 43, 5010–5013.
- [29] A. D’Aleo, A. Picot, A. Beeby, J. A. Gareth Williams, B. Le Guenic, C. Andraud, O. Maury, *Inorg. Chem.* **2008**, 47, 10258–10268.
- [30] G. S. Kottas, M. Mehlstaubl, R. Froehlich, L. De Cola, *Eur. J. Inorg. Chem.* **2007**, 3465–3468.
- [31] G. Zucchi, O. Maury, P. Thuery, F. Gumy, J.-C. G. Bünzli, M. Ephritikhine, *Chem. Eur. J.* **2009**, DOI: 10.1002/chem.200901517.
- [32] N. M. Shavaleev, R. Scopelliti, F. Gumy, J.-C. G. Bünzli, *Inorg. Chem.* **2009**, 48, 5611–5613.
- [33] C. Piguet, B. Bocquet, G. Hopfgartner, *Helv. Chim. Acta* **1994**, 77, 931–942.
- [34] N. André, T. B. Jensen, R. Scopelliti, D. Imbert, M. Elhabiri, G. Hopfgartner, C. Piguet, J.-C. G. Bünzli, *Inorg. Chem.* **2004**, 43, 515–529.
- [35] “Self-Assembled Lanthanide Helicates: From Basic Thermodynamics to Applications”: C. Piguet, J.-C. G. Bünzli in *Handbook on the Physics and Chemistry of Rare Earths, Vol. 40* (Eds.: K. A. Gschneidner, Jr., J.-C. G. Bünzli, V. K. Pecharsky), Elsevier, Amsterdam, **2010**, Chapter 247, pp. 301–553.
- [36] N. M. Shavaleev, R. Scopelliti, F. Gumy, J.-C. G. Bünzli, *Inorg. Chem.* **2009**, 48, 6178–6191.
- [37] D. Yang, D. Fokas, J. Li, L. Yu, C. Baldino, *Synthesis* **2005**, 47–56.
- [38] R. Dodd, M. Le Hyaric, *Synthesis* **1993**, 295–297.
- [39] L. C. Thompson, Complexes in *Handbook on the Physics and Chemistry of Rare Earths, Vol. 3* (Eds.: K. A. Gschneidner, Jr., L. Eyring), North Holland, Amsterdam, **1979**, Chapter 25, pp. 209–297.
- [40] I. D. Brown, *Acta Crystallogr. Sect. A* **1992**, 48, 553–572.
- [41] A. Trzesowska, R. Kruszynski, T. J. Bartczak, *Acta Crystallogr. Sect. A* **2004**, 60, 174–178.
- [42] A. Trzesowska, R. Kruszynski, T. J. Bartczak, *Acta Crystallogr. Sect. A* **2005**, 61, 429–434.

- [43] J.-C. G. Bünzli, S. V. Eliseeva in *Springer Series on Fluorescence, Vol. 7, Lanthanide Spectroscopy, Materials, and Bio-applications* (Eds.: P. Hänninen, H. Härmä), Springer, Berlin, **2010**, Chapter 2.
- [44] M. Latva, H. Takalo, V. M. Mikkala, C. Matachescu, J.-C. Rodriguez-Ubis, J. Kankare, *J. Lumin.* **1997**, *75*, 149–169.
- [45] J.-C. G. Bünzli, B. Klein, D. Wessner, N. W. Alcock, *Inorg. Chim. Acta* **1982**, *59*, 269–274.
- [46] M. H. V. Werts, R. T. F. Jukes, J. W. Verhoeven, *Phys. Chem. Chem. Phys.* **2002**, *4*, 1542–1548.
- [47] CrysAlis PRO, Oxford Diffraction Ltd., Yarnton, Oxfordshire, **2009**.
- [48] A. J. M. Duisenberg, L. M. J. Kroon-Batenburg, A. M. M. Schreurs, *J. Appl. Crystallogr.* **2003**, *36*, 220–229.
- [49] R. H. Blessing, *Acta Crystallogr. Sect. A* **1995**, *51*, 33–38.
- [50] G. Sheldrick, *Acta Crystallogr. Sect. A* **2008**, *64*, 112–122.
- [51] A. L. Spek, PLATON. A Multipurpose Crystallographic Tool, Utrecht University, Utrecht, **2008**.

Received: July 19, 2009

Published online: September 16, 2009